REGULAR ARTICLE

blood advances

Heterozygous mutation *SLFN14 K208N* in mice mediates species-specific differences in platelet and erythroid lineage commitment

Rachel J. Stapley,[1] Christopher W. Smith,[1] Elizabeth J. Haining,[1] Andrea Bacon,[2] Sian Lax,[3] Vera P. Pisareva,[4] Andrey V. Pisarev,[4] Steve P. Watson,[1,5] Abdullah O. Khan,[1] and Neil V. Morgan[1]

[1]Institute of Cardiovascular Sciences, College of Medical and Dental Sciences, [2]MRC Centre for Immune Regulation, Transgenics Facility, and [3]Institute of Cancer and Genomic Sciences, College of Medical and Dental Sciences, University of Birmingham, Edgbaston, United Kingdom; [4]Department of Cell Biology, SUNY Downstate Health Sciences University, Brooklyn, NY; and [5]Centre of Membrane Proteins and Receptors, Universities of Birmingham and Nottingham, Midlands, United Kingdom

Key Points

- Heterozygous mutations in the *SLFN14* AAA domain cause species-specific differences in platelet and erythroid lineage commitment.
- *SLFN14*$^{K208N/+}$ mice display pronounced microcytic erythrocytosis and anemia resulting from defective red blood cell formation.

Schlafen 14 (SLFN14) has recently been identified as an endoribonuclease responsible for cleaving RNA to regulate and inhibit protein synthesis. Early studies revealed that members of the *SLFN* family are capable of altering lineage commitment during T-cell differentiation by using cell-cycle arrest as a means of translational control by RNase activity. *SLFN14* has been reported as a novel gene causing an inherited macrothrombocytopenia and bleeding in human patients; however, the role of this endoribonuclease in megakaryopoiesis and thrombopoiesis remains unknown. To investigate this, we report a CRISPR knock-in mouse model of *SLFN14 K208N* homologous to the K219N mutation observed in our previous patient studies. We used hematological analysis, in vitro and in vivo studies of platelet and erythrocyte function, and analysis of spleen and bone marrow progenitors. Mice homozygous for this mutation do not survive to weaning age, whereas heterozygotes exhibit microcytic erythrocytosis, hemolytic anemia, splenomegaly, and abnormal thrombus formation, as revealed by intravital microscopy, although platelet function and morphology remain unchanged. We also show that there are differences in erythroid progenitors in the spleens and bone marrow of these mice, indicative of an upregulation of erythropoiesis. This *SLFN14* mutation presents distinct species-specific phenotypes, with a platelet defect reported in humans and a severe microcytic erythrocytosis in mice. Thus, we conclude that *SLFN14* is a key regulator in mammalian hematopoiesis and a species-specific mediator of platelet and erythroid lineage commitment.

Introduction

Endoribonucleases are a family of proteins responsible for cleaving RNA to regulate and inhibit protein synthesis.[1] The Schlafen (SLFN) family of proteins/genes is made up of 10 mouse and 6 human *SLFN* genes, all of which possess a characteristic AAA domain coding for DNA helicases, transcription regulators, protein folding regions, and a distinctive SLFN box of unknown function.[2] SLFN proteins are divided into 3 subgroups and are highly homologous, classified based on their increasing length. Subgroups II and III contain the aforementioned regions and a SWADL region, whereas subgroup III also possesses an additional helicase region ~ 400 aa.[2-5]

Reported roles for the SLFN family of proteins include translational control by RNase activity (SLFN14), transfer RNA cleavage as part of the DNA damage response in tumor cells, and T-cell lineage and commitment (SLFN1).[6] Recently, *SLFN14* mutations have been reported in 5 unrelated families worldwide who present with macrothrombocytopenia and associated excessive bleeding.[7-11] Patients

Submitted 20 May 2020; accepted 1 December 2020; published online 19 January 2021. DOI 10.1182/bloodadvances.2020002404.

Data sharing requests should be sent to Neil V. Morgan (n.v.morgan@bham.ac.uk).

The full-text version of this article contains a data supplement.

with these mutations have a platelet function defect in response to adenosine diphosphate, collagen, and PAR1-peptide and decreased platelet adenosine triphosphate secretion.[7] Further investigation discovered that SLFN14 colocalizes with ribosomes and causes endoribonucleolytic degradation of ribosomal RNA in cells.[12] These data, coupled with expression data from several databases, suggest that *SLFN14* is responsible for cleavage and regulation of critical RNAs in megakaryocytic and erythroid differentiation. Regulatory RNAs are thought to be critical in hematopoietic lineage commitment, with unique RNA signatures reported in multipotent and bipotent progenitors.[13-15] Pisareva et al revealed that SLFN14 is associated with cleaving RNA and ribosome-bound messenger RNA (mRNA) in an Mg^{2+}-dependent and nucleotide triphosphate (NTP)–independent manner.[16] Recent evidence in primary human cells from platelet and erythroid lineages suggests that SLFN14 may function in a similar way in cleaving RNA from the ribosomal unit prior to splitting, influencing hemoglobin production during blood cell development.[17]

Despite these insights, the mechanistic role of *SLFN14* in megakaryocyte (MK) development and hemostasis is unknown. To address this, we generated a global CRISPR-mediated knock-in (KI) mouse model of the patient mutation K219N missense substitution (mouse K208N homolog), which is known to cause thrombocytopenia, and investigated its overall role in hematopoiesis and platelet function. Homozygous KI mice for this mutation ($SLFN14^{K208N/K208N}$) did not survive to weaning and, similarly, *SLFN14* mutations identified in humans are all of a heterozygous nature; therefore, heterozygous mice were used in all experiments compared with litter-matched wild-type controls ($SLFN14^{K208N/+}$ and $SLFN14^{+/+}$, respectively). We investigated the *SLFN14 K208N* mutation through hematological analysis, platelet activation, function, and its overall role in hematopoiesis. $SLFN14^{K208N/+}$ mice showed significant differences from $SLFN14^{+/+}$ mice in gross hematological analyses. However, unlike the human variants, these mice demonstrate a major defect in erythropoiesis but not megakaryopoiesis or thrombopoiesis.

Differences in the consequences of this missense mutation suggest that *SLFN14* is a species-specific regulator of platelet and erythroid lineage commitment. In humans, the mutation causes a defect in thrombopoiesis, whereas a homologous missense mutation in mice causes a significant defect in erythropoiesis. $SLFN14^{K208N/+}$ mice present with pronounced microerythrocytosis, hemolytic anemia, splenomegaly, and abnormal thrombus formation in vivo.

Materials and methods

Mice

A *SLFN14 K208N*–KI mouse was generated in-house using CRISPR-Cas9 gene editing. All mice were generated on a C57BL/6J background and were bred in heterozygote/wild-type pairs. Animal care and welfare were in accordance with United Kingdom Home Office regulations and the use of Animals (Scientific Procedures) Act 1986. Animals were housed at the Biomedical Services Unit at the University of Birmingham.

Genotyping

All mice were genotyped in-house using DNA extraction from mouse ear clips (DNeasy Blood & Tissue Kits; Qiagen, Manchester, United Kingdom). Polymerase chain reaction (PCR) and Sanger sequencing were used to identify *SLFN14 K208N*–KI mice following the procedure and conditions outlined in supplemental Tables 1 and 2.

Flow cytometry

Flow cytometry was performed on a BD Accuri C6 flow cytometer, and results were analyzed using BD Accuri C6 software. Flow cytometry antibodies are listed in supplemental Tables 4.

Platelet preparation

Mice were exsanguinated under terminal anesthesia by isoflurane/O_2 (5%) gas. Blood was drawn from the inferior vena cava, using a 25-gauge needle, into 1:10 (volume-to-volume ratio) acid citrate dextrose anticoagulant. Washed platelets were prepared as described in supplemental Material.

Light transmission aggregometry

Washed platelet counts were normalized to 2×10^8/mL with Tyrode's-HEPES buffer. Aggregation in 300 μL of platelets was measured using a lumi-aggregometer (Chrono-Log, Havertown, PA) at 37°C under stirring conditions (1200 rpm) for 6 minutes post–agonist addition.

Platelet spreading

Washed platelets at 2×10^7/mL were incubated for 45 minutes on collagen-coated (10 μg/mL) and fibrinogen-coated (100 μg/mL) coverslips under resting or preactivated conditions (0.1 U/mL thrombin). Adhered cells were fixed with 10% formalin, permeabilized, and stained with Alexa Fluor 488–conjugated phalloidin. Images were captured on a Zeiss Epifluorescence microscope and analyzed using a semiautomated machine learning–based workflow.[18,19]

Hemostasis assay

All experiments were double blinded and conducted on 20 to 29g $SLFN14^{K208N/+}$ and litter-matched wild-type mice. Mice were anesthetized using isoflurane/O_2 (5%) gas, and 2 to 3 mm of tail tip was excised using a sterile razor blade and placed in prewarmed saline (37°C). Time until first cessation of bleeding was recorded.

Clot retraction

Platelet-rich plasma (PRP) from $SLFN14^{K208N/+}$ and $SLFN14^{+/+}$ mice was adjusted to a final concentration of 2×10^8/mL using platelet-poor plasma and Tyrode's-HEPES buffer supplemented with 2mM $CaCl_2$, as previously described.[20] Erythrocytes were added for visualization, and clot formation was stimulated by 1 U/mL thrombin. Clots were monitored every 30 minutes for 2 hours, and clot weight and volume were calculated.

In vivo thrombosis assays

Laser-induced injury of cremaster arterioles and $FeCl_3$-induced injury of carotid arteries were performed and analyzed as previously described.[21]

Histological analysis

Spleens and decalcified bones were embedded in paraffin wax and sectioned at 5 μm prior to staining with hematoxylin and eosin (H&E) and Perls Prussian blue. Sections were scanned using a Zeiss Axio ScanZ1 slide scanner (Carl Zeiss Ltd., Cambridge, UK). The number of MKs was counted in 10 fields of view taken

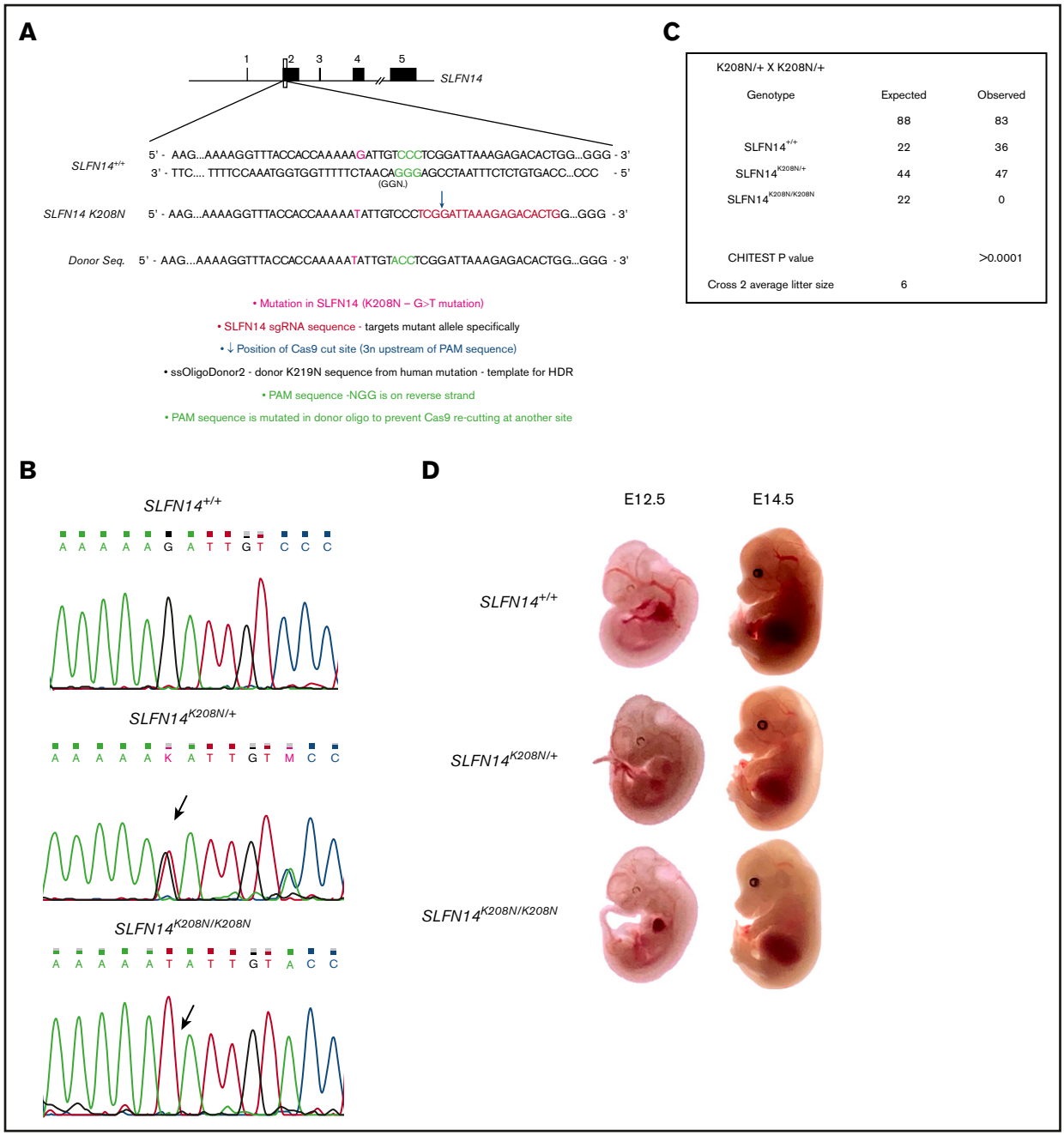

Figure 1. Generation of *SLFN14 K208N* mice using CRISPR-Cas9 gene editing and embryo development. (A) Schematic diagram of CRISPR-Cas9 gene-editing mechanism using human K219N donor oligonucleotide. (B) Wild-type, *SLFN14*$^{K208N/+}$, and *SLFN14*$^{K208N/K208N}$ traces showing successful KI of G>T missense mutation (arrow). (C) Non-Mendelian inheritance pattern of *SLFN14 K208N* mice. χ^2 square analysis shows significant deviation from Mendelian inheritance and prewean loss of homozygotes ($P < .0001$). Data are taken from 15 litters of heterozygote/heterozygote (cross 2) breeding pairs. (D) Representative images of backlit embryos taken at E12.5 and E14.5 (original magnification ×3). n = 3 to 9 embryos per genotype.

from 2 femur sections and 1 spleen section per mouse. Sectioning and image analysis were performed double blinded.

Spleen and bone marrow progenitor flow cytometry

Spleens were homogenized and whole bone marrow was flushed from mouse femurs and tibias in 1% fetal bovine serum and 2 mM EDTA in phosphate-buffered saline. Cells were filtered through a 70-μm cell strainer and stained with antibodies as per supplemental Table 4. A total of 50 000 events was collected using a BD Accuri C6 flow cytometer and gated to eliminate dead and cell doublets. Cells were imaged on poly-L-lysine coated coverslips using a Zeiss LSM880 confocal microscope.

Statistical analysis

Data are presented as mean ± standard error of the mean (SEM), unless stated otherwise. A Student *t*-test and 2-way analysis of

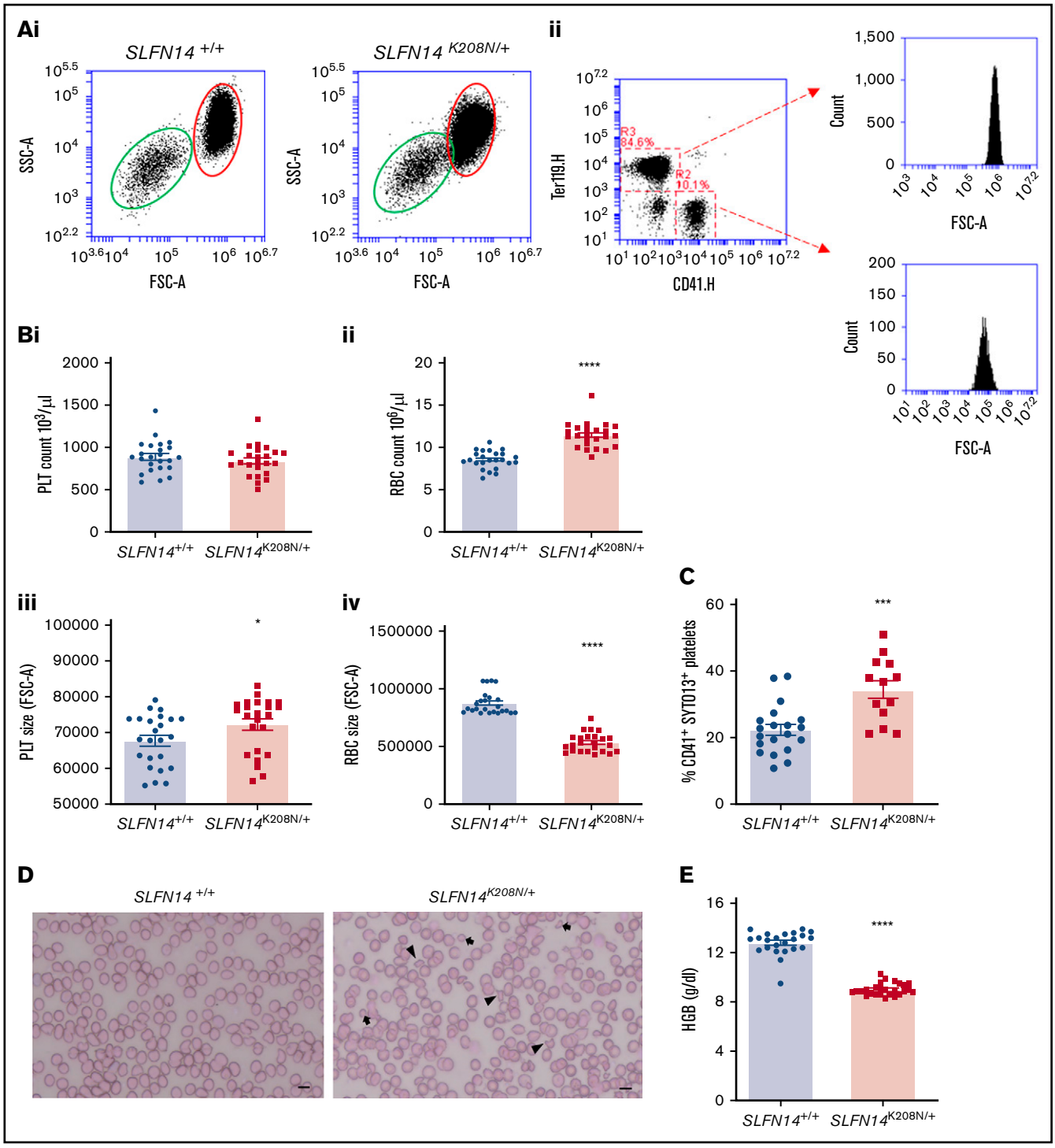

Figure 2. Hematological analysis of *SLFN14*$^{K208N/+}$ mice. (A) Flow cytometry–based counting of platelets and erythrocytes. (Ai) Flow cytometry forward scatter (FSC) and side scatter (SSC) plots showing size overlap of erythrocyte (red oval) and platelet (green oval) populations. (Aii) Gating method shown for double stain using CD41 (R2) and Ter119 (R3). Representative plots of n = 18 mice per genotype. (B) Platelet (PLT) (i) and erythrocyte (RBC) (ii) count and platelet (iii) and erythrocyte (iv) size from flow cytometry–based counting. Data are mean ± standard error of the mean (SEM); n = 18 mice per genotype. (C) Immature platelet fraction in *SLFN14*$^{K208N/+}$ mice. CD41^{+} platelets were gated, and the immature platelet population was assessed by SYTO13 staining. Data are mean ± SEM; n = 13 to 20 mice per genotype. (D) Whole blood smears from wild-type and *SLFN14*$^{K208N/+}$ mice. Blood smears were stained with H&E histological stain to view blood cell size and morphology. Poikilocytes (irregularly shaped cells; arrowheads) and microcytes (arrows) are shown. Representative images of n = 6 or 7 mice per genotype. Scale bar, 10 µm. (E) *SLFN14*$^{K208N/+}$ mice are anemic. Hemoglobin levels were measured by an automated hematology analyzer in *SLFN14*$^{K208N/+}$ mice and wild-type controls. Data are mean ± SEM; n = 23 to 26 mice per genotype. *$P < .05$, ***$P < .001$, ****$P < .0001$.

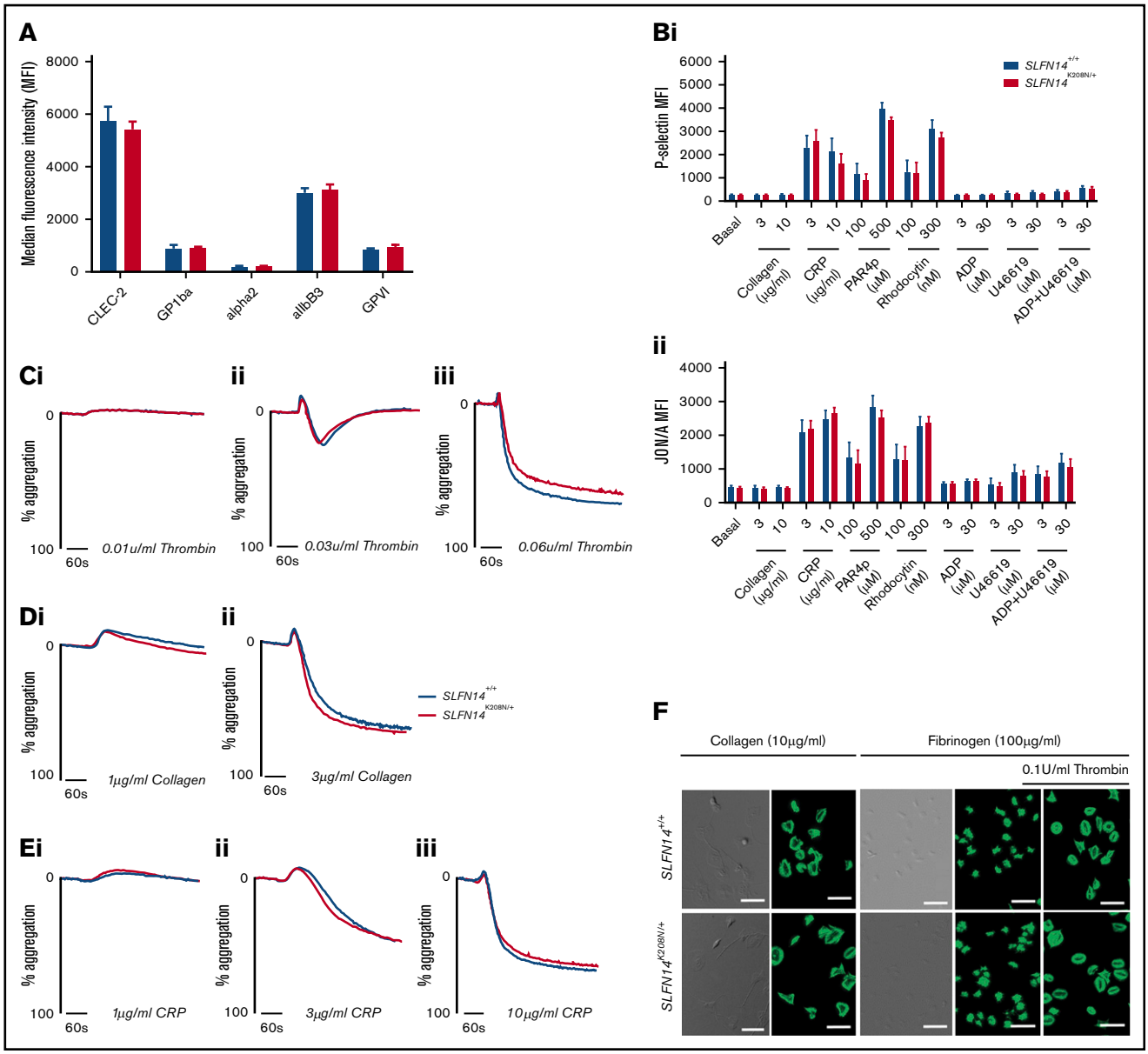

Figure 3. In vitro assessment of platelet function in *SLFN14*$^{K208N/+}$ mice. (A) Resting platelet surface glycoprotein expression levels. GP1ba^{+} platelets were costained for the indicated surface receptors in whole blood. Median fluorescence intensity (MFI) from 4 to 6 mice per genotype. Data are mean ± standard error of the mean (SEM); significance was assessed using Welch's *t* test for multiple comparisons. (B) P-selectin (i) and activated αIIbβ3 (JON/A) (ii) expression on *SLFN14*$^{K208N/+}$ mouse platelets in response to the indicated agonist stimulation. Data are MFI (mean ± SEM) for 9 mice per genotype per condition. Significance was assessed by Sidak's 2-way analysis of variance. (C) Platelet reactivity in washed platelets in response to 0.01 U/mL (i), 0.03 u/mL (ii), or 0.06 U/mL (iii) thrombin. (D) Platelet reactivity in washed platelets in response to 1 μg/mL (i) or 3 μg/mL (ii) collagen. (E) Platelet reactivity in washed platelets in response 1 μg/mL (i), 3 μg/mL (ii), or 10 μg/mL (iii) collagen-related peptide. Representative traces of 3 to 6 mice per genotype per condition are shown. (F) Platelet spreading and adhesion in *SLFN14*$^{K208N/+}$ mice. *SLFN14*$^{K208N/+}$ platelets spread on collagen or fibrinogen under resting and thrombin-preactivated conditions (0.1 U/mL thrombin). Representative differential interference contrast and fluorescent phalloidin–stained images are shown from 3 mice per genotype/condition. Scale bar, 10 μm.

variance were used for platelet activation, and a Mann-Whitney *U* test was used for in vivo analysis, with $P < .05$ deemed significant. All analyses were conducted using GraphPad Prism software (v8.4).

Animal care and welfare were in accordance with United Kingdom Home Office regulations and the use of Animals in Scientific Procedures Act 1986 under Project License number P53D52513 (to N.V.M.).

Results

SLFN14 K208N homozygotes do not survive to weaning because of severe anemia

An in-house CRISPR-KI model was developed using homology directed repair (HDR). Human oligonucleotide donor templates of the K219N mutation were coinjected with single guide RNA as per the CRISPR-Cas9 mechanism (Figure 1A). This resulted in the

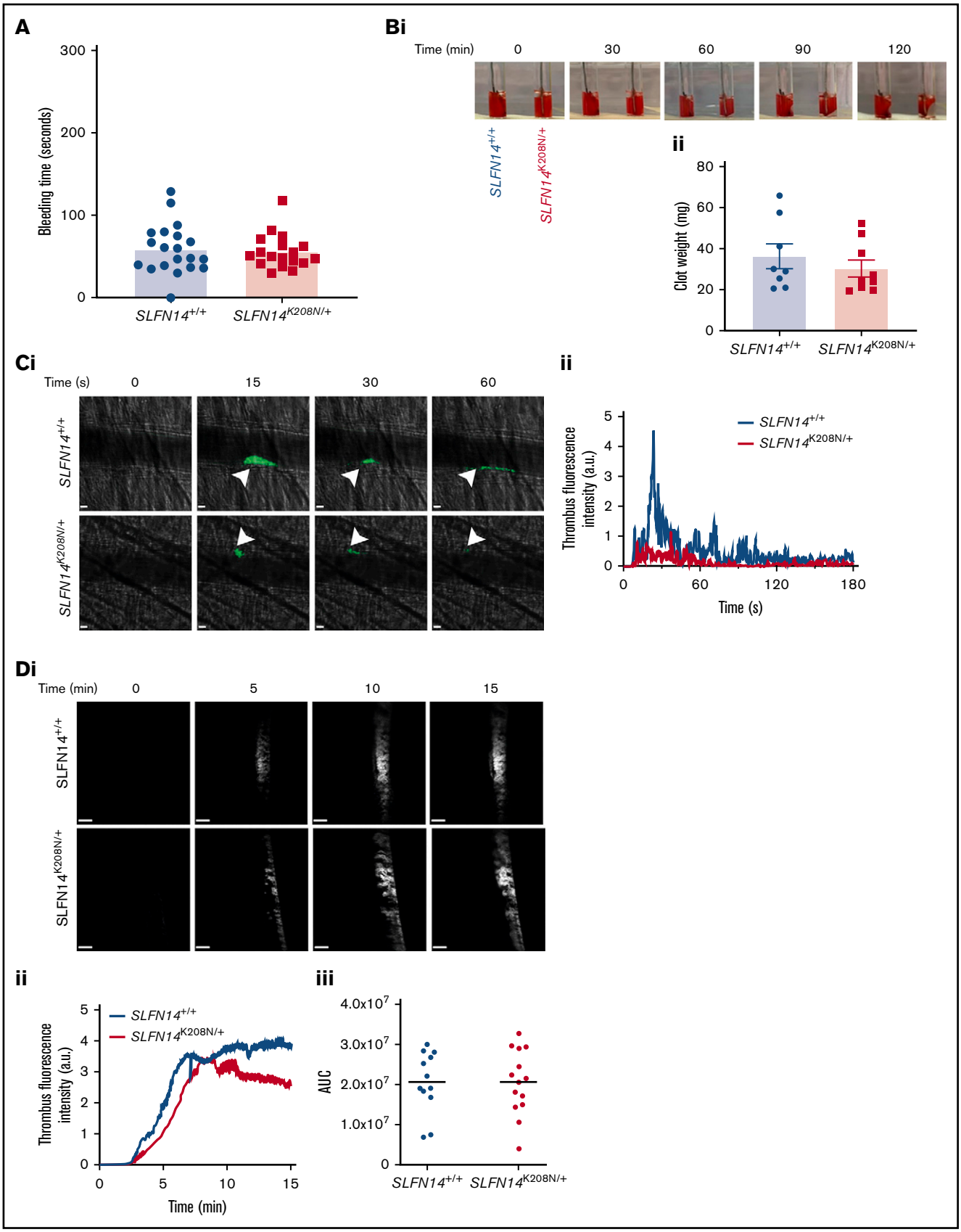
A
Bleeding time (seconds)
300
200
100
0
SLFN14+/+
SLFN14K208N/+
Bi
Time (min)
0
30
60
90
120
SLFN14+/+
SLFN14K208N/+
ii
Clot weight (mg)
80
60
40
20
0
SLFN14+/+
SLFN14K208N/+
Ci
Time (s)
0
15
30
60
SLFN14+/+
SLFN14K208N/+
ii
Thrombus fluorescence intensity (a.u.)
SLFN14+/+
SLFN14K208N/+
Time (s)
0
60
120
180
Di
Time (min)
0
5
10
15
SLFN14+/+
SLFN14K208N/+
ii
Thrombus fluorescence intensity (a.u.)
SLFN14+/+
SLFN14K208N/+
Time (min)
iii
AUC
4.0x10^7
3.0x10^7
2.0x10^7
1.0x10^7
0
SLFN14+/+
SLFN14K208N/+

Figure 4.

G>T substitution and subsequent K208N amino acid change. Sanger sequencing was used to genotype mice, with Figure 1B showing successful KI of the mutation. A χ^2 analysis of heterozygote/heterozygote breeding pairs shows significant deviation from Mendelian inheritance, with ~25% of offspring lost preweaning ($P < .0001$; Figure 1C). The average prewean loss was 25% across 15 litters, the same proportion of expected homozygote offspring according to Mendel's law (supplemental Table 3). To assess embryonic lethality, embryos were gathered for observation and genotyping at 12.5 and 14.5 days post–vaginal plug. At embryonic day 12.5 (E12.5), *SLFN14*$^{K208N/+}$ mice were not different from wild-type littermates. However, *SLFN14*$^{K208N/K208N}$ embryos were significantly paler, with less-defined vasculature (Figure 1D). E14.5 *SLFN14*$^{K208N/K208N}$ embryos were much more pale, with substantially less vascular definition than that seen in the other genotypes (Figure 1D). No *SLFN14*$^{K208N/K208N}$ mice survived to weaning for genotyping; therefore, we can deduce that if *SLFN14*$^{K208N/K208N}$ pups do survive beyond the critical fetal liver stage at day 14.5, they die shortly after birth. Therefore, in parallel with K219N heterozygous patients, *SLFN14 K208N* heterozygotes were used in analyses.

SLFN14$^{K208N/+}$ mice have microcytic erythrocytosis, poikilocytosis, and anemia

SLFN14$^{K219N/+}$ patients exhibit macrothrombocytopenia; however, we did not observe any difference in platelet count in homologous *SLFN14*$^{K208N/+}$ mice, but we did detect an increase in size using a flow cytometry counting assay and single positive events of CD41 and Ter119–stained cells (Figure 2A,Bi-ii; $P < .0001$). Contrary to the patient mutation, for which no effect on erythrocyte production or function was reported, *SLFN14*$^{K208N/+}$ mice exhibit microcytic erythrocytosis, an increase in erythrocyte count accompanied by a reduction in size (Figure 2Biii-iv). We did not observe any difference in leukocyte counts between genotypes (data not shown).

SLFN14$^{K219N/+}$ patients have a high immature platelet fraction (IPF).[7] We assessed IPF in *SLFN14*$^{K208N/+}$ mice using a flow cytometry method and nucleic acid stain SYTO13, which was recently reported to be a more specific marker than its predecessor, Thiazole orange.[22] A 15% increase in the proportion of CD41$^+$ SYTO13$^+$ cells was observed in *SLFN14*$^{K208N/+}$ mice compared with *SLFN14*$^{+/+}$ controls (Figure 2C; $P = .0003$). Combined with the observed increase in platelet size, these data indicate an increase in the proportion of immature platelets in *SLFN14*$^{K208N/+}$ mice.

Whole blood smears from *SLFN14*$^{K208N/+}$ mice show irregularly shaped smaller erythrocytes (poikilocytes and microcytes) compared with the characteristic plump-shaped cells observed in wild-type controls (Figure 2D). This microcytosis is accompanied by lower hemoglobin levels in *SLFN14*$^{K208N/+}$ mice (Figure 2E).

These results and previous work in T-cell lineage commitment studies identify *SLFNs* as key drivers in species-dependent hematopoietic lineage commitment. In this case, we observe *SLFN14* mutations causing distinct differences in platelet and erythrocyte production and morphology.[3,6]

SLFN14$^{K208N/+}$ mice exhibit normal platelet function in response to major agonists

No alteration in major glycoprotein receptor levels was observed in *SLFN14*$^{K208N/+}$ platelets (Figure 3A). Platelet activation was assessed by flow cytometry, and both genotypes displayed similar α-granule secretion (P-selectin) and integrin αIIbβ3 activation (JON/A) in response to agonists at varying doses (Figure 3B). Platelet function in *SLFN14*$^{K208N/+}$ mice was assessed using light transmission aggregometry. *SLFN14*$^{K208N/+}$ mice display normal platelet function compared with their wild-type littermates in response to the agonists thrombin, collagen, and collagen-related peptide (Figure 3C-E), which are mediated by G protein–coupled receptors and ITAM/receptor tyrosine kinase, and are the 2 main types of activation receptors in platelets.

We next investigated platelet adhesion and spreading on collagen- or fibrinogen-coated surfaces. Under resting and preactivated conditions, no difference in adhesion or cytoskeletal remodeling was observed in *SLFN14*$^{K208N/+}$ platelets (Figure 3F).[18,19]

Hemostasis and thrombosis in *SLFN14*^{K208N} mice

SLFN14 patients were recruited to studies based on their bleeding phenotypes. To establish whether *SLFN14* transgenic mice had a bleeding phenotype, 2 to 3 mm of tail tip was excised, and time to bleeding cessation in prewarmed (37°C) saline was measured. No difference was observed in either genotype, indicating that platelets retain normal function, and abnormal erythrocytes do not impact hemostasis in this model (Figure 4A).

Clot retraction was also investigated in PRP to assess αIIbβ3-mediated platelet function. No visual difference was observed during the time course, and final mean clot weight of 36.0 mg and 30.0 mg for *SLFN14*$^{+/+}$ and *SLFN14*$^{K208N/+}$ mice, respectively, was not significantly different (Figure 4B). This supports our findings that platelet function is maintained and that the *SLFN14 K208N* mutation in mice does not lead to platelet function defects.

Thrombus formation was assessed in vivo by laser- and $FeCl_3$-induced injury models. Following laser injury, *SLFN14*$^{K208N/+}$ mice

Figure 4. Functional role of *SLFN14* in thrombosis. (A) Tail bleeding time assay. Two to 3 millimeters of tail was removed, and bleeding time until first stop was measured. Each data point represents 1 animal; n = 18 to 20 mice per genotype. (B) Clot retraction of *SLFN14*$^{K208N/+}$ mouse platelets in PRP. Clots were formed by stimulating 2×10^8 platelets per milliliter with 0.1 U/mL thrombin; monitoring took place for 2 hours. Representative images (Bi) and final clot weight (Bii). Data are mean ± SEM; n = 8 or 9 mice per genotype. (C) Laser-induced thrombus formation in vivo. (Ci) Representative composite brightfield and fluorescence images of thrombus formation. Mice were injected with anti-GPIbβ DyLight488 (0.1 μg/g body weight). Arterioles of the cremaster muscle were subsequently injured by laser (arrowheads) and thrombi fluorescence was measured. Scale bars, 10 μm. (Cii) Graph showing median integrated thrombus formation fluorescence intensity in arbitrary units (a.u.) for 31 or 32 injuries in 4 mice per genotype. (D) $FeCl_3$-induced thrombus formation. Mice were injected with DyLight488-conjugated anti-GPIbβ antibody (0.1 μg/g body weight), and the carotid artery was subsequently injured with 10% $FeCl_3$ solution for 3 minutes. (Di) Representative fluorescence images of platelets (GPIbβ). Scale bars, 200 μm. (Dii) Graph showing median integrated thrombus fluorescence. (Diii) Area under the curve (AUC) of the integrated fluorescence density (in a.u). Data are mean; n = 11 or 12 mice per genotype. See supplemental Videos 3 and 4 for wild-type and mutants, respectively.

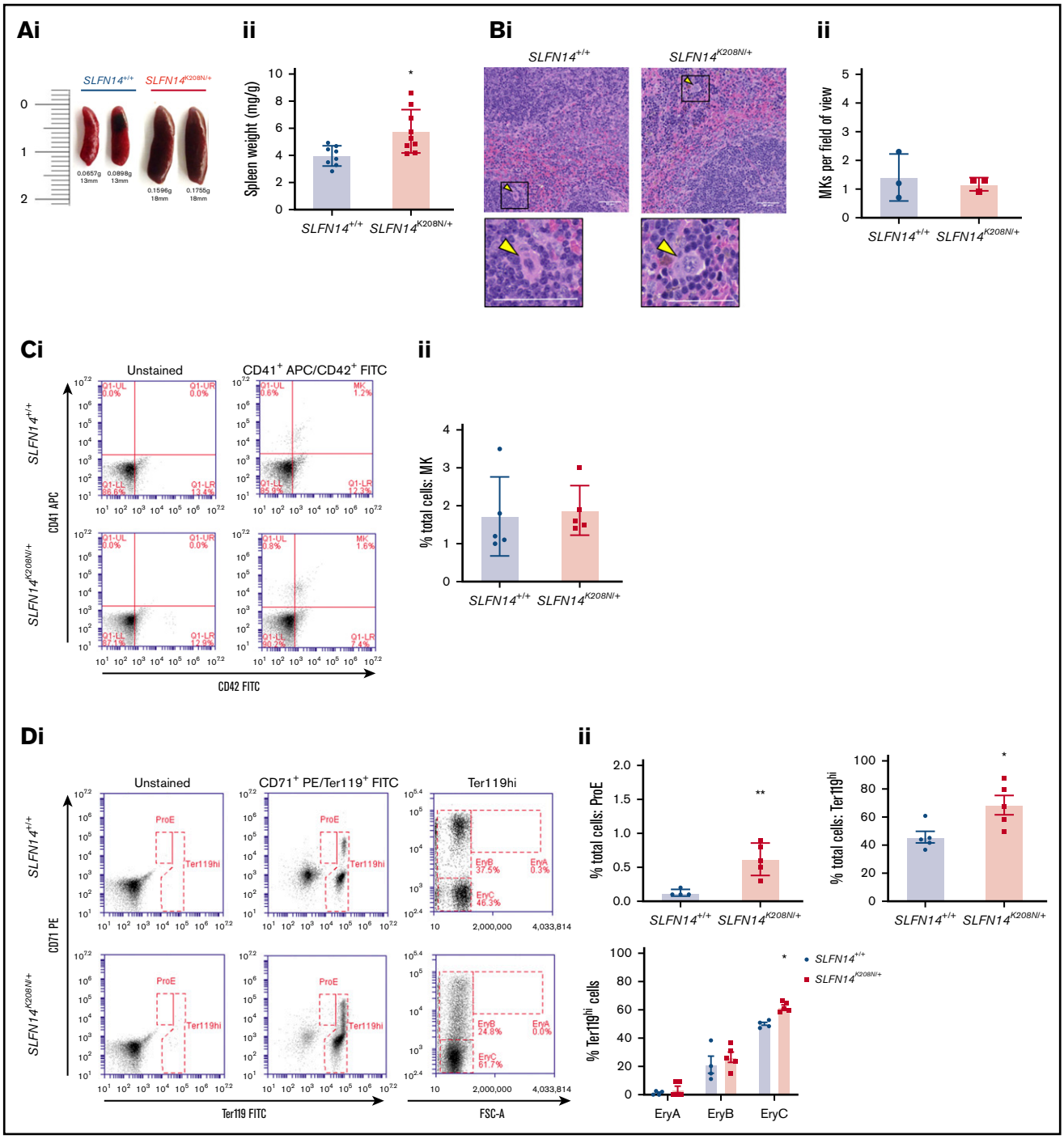

Figure 5. *SLFN14*$^{K208N/+}$ mice exhibit splenomegaly and extramedullary erythropoiesis. (Ai) Representative images of spleens from *SLFN14*$^{K208N/+}$ and *SLFN14*$^{+/+}$ mice. (Aii) Normalized spleen weight. Spleen weight/body weight (mg/g) from 8 or 9 mice per genotype. (Bi) Representative images of H&E-stained spleen sections from *SLFN14*$^{K208N/+}$ and wild-type controls. Arrowheads indicate MKs. Scale bars, 50 μm. (Bii) Quantification of MK number per field of view. n = 3 mice per genotype, 10 or 11 fields of view per tissue sample. Analysis was conducted blind. (C) Quantification of MKs in spleen. (Ci) MK staining: MKs were identified by CD41 (αIIb) allophycocyanin (APC) and CD42 (GPIb) fluorescein isothiocyanate (FITC) double staining. (Cii) Proportion of MKs in spleen flow cytometry. (D) Quantification of erythroid progenitors in spleen. (Di) ProE staining: ProEs were identified as double-positive CD71 (transferrin receptor 1) phycoerythrin (PE) and Ter119 FITC cells (ProE gate). (Dii) Quantification of ProEs, increased Ter119^{+} cell population in *SLFN14*$^{K208N/+}$ mice, and profile of Ter119^{hi} cells by EryA, EryB, and EryC gates. (E) Quantification of MK-EB–primed MEPs in the spleen: MEPs were identified as a small population positive for CD71 (transferrin receptor 1) PE and CD41 (αIIb) APC (MEP). (Ei) Flow cytometry plots show a slight, but insignificant, increase in MEP cell numbers in *SLFN14 K208N* mice compared with wild-type. (Eii) MEP quantification. All spleen flow cytometry data and quantification are representative of 4 or 5 mice per genotype/staining condition. (F) Representative images of hemosiderin deposits in spleen sections of wild-type and *SLFN14*$^{K208N/+}$ mice highlighted by Perls Prussian blue staining. Scale bars, 50 μm. n = 3 mice per genotype. *$P < .05$, **$P < .01$, Student *t* test.

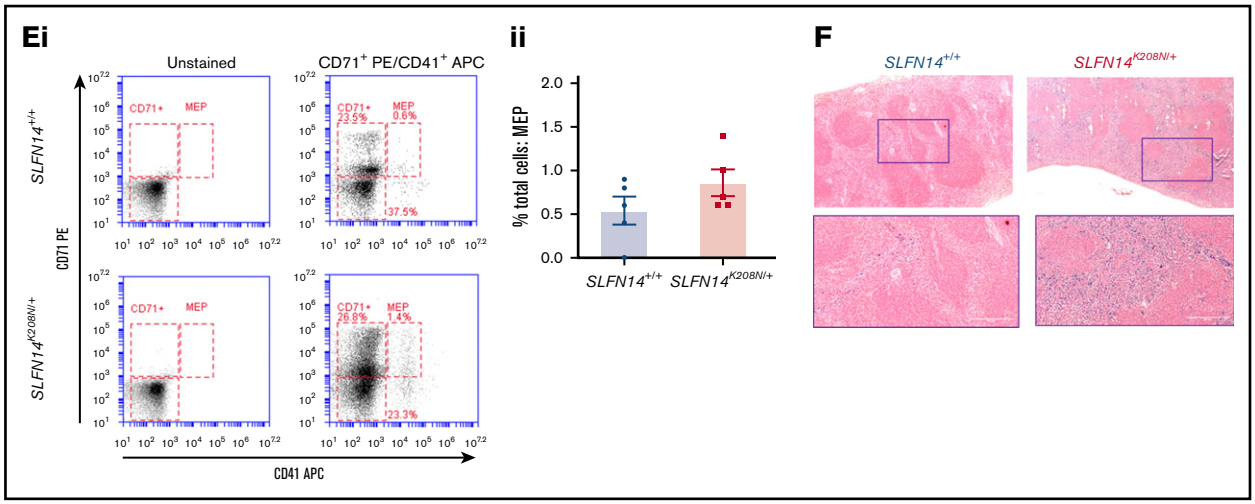

Figure 5. (Continued).

form thrombi at a similar rate to *SLFN14*$^{+/+}$ controls, although they are smaller, with fewer platelets recruited, and embolize more quickly than do those in littermate controls (Figure 4C; supplemental Videos 1 and 2, respectively). $FeCl_3$ injury to the carotid artery resulted in occlusive thrombus formation in both genotypes (Figure 4D; supplemental Videos 3 and 4). Monitoring the accumulation of fluorescently labeled platelets shows that *SLFN14*$^{K208N/+}$ mice form thrombi at a slightly slower rate and have a tendency for reduced stability, although these were not statistically different from littermate controls (Figure 4Dii-iii). Ultimately, thrombus formation and stability defects in *SLFN14*$^{K208N/+}$ mice are driven by the involvement of other blood cells; together with in vitro platelet function studies, these findings suggest that *SLFN14 K208N* has only a minor role in mouse platelets.

Splenomegaly in *SLFN14*$^{K208N/+}$ mice is due to extramedullary erythropoiesis, the accumulation of mature erythrocytes, and hemolytic anemia

The spleen acts as a major site for filtering and clearance of blood from the circulation. In classical findings of clearance, platelets undergo phagocytosis controlled by their immunoglobulin G–coated surfaces, rendering Fc receptor–directed clearance by macrophages in the spleen.[23] The spleen can also act as an additional site of hematopoiesis in the event of myelofibrosis or bone marrow scarring in certain pathologies.[24] We investigated the spleen to assess differences in blood cell production and clearance. After controlling for body weight, spleens of *SLFN14*$^{K208N/+}$ mice were significantly larger with regard to weight and size compared with those from *SLFN14*$^{+/+}$ littermates (Figure 5A). MK counts from histology sections in the spleen were normal, and the proportion of MKs was unchanged between genotypes by flow cytometry analysis (Figure 5B-C).

Using a similar gating strategy to Koulnis et al, we used CD71 (early erythroid progenitor marker) and Ter119 (mature erythroid marker) to detect erythroid cells and categorized Ter119^{hi} cells according to size (Figure 5Di).[25] There was a significant increase in the proportion of proerythroblasts (ProEs) in heterozygotes (CD71$^+$/Ter119$^+$; Figure 5Dii). In these spleens, we did not detect any EryA progenitors in either genotype (Figure 5D). However, despite fairly consistent proportions of Ter119^{hi} cells between genotypes, we observed a difference in the distribution and greater spread of CD71$^+$ cells within the EryB gate and an increase in EryCs (most mature erythroid cells) in heterozygotes that was suggestive of erythroid maturation from the intermediate progenitor within the spleen (Figure 5D). Gating strategy for spleen flow cytometry is detailed in supplemental Figure 1.

Our flow cytometry progenitor panel aimed to detect megakaryocyte-erythroid progenitors (MEPs). Consistent with previous findings by Psaila et al, we identified 2 subpopulations by differential expression of CD71 and a small MEP population by coexpression of CD41.[26] CD71$^+$/CD41$^+$ cells were rare in these samples, consistent with previous findings, although we did detect an almost threefold increase in MEPs in *SLFN14*$^{K208N/+}$ mice than in wild-types[26] (Figure 5E). In addition, we observed a greater spread of cells within our CD71$^+$ population in contrast to the more clustered appearance in controls.

We discovered substantial hemosiderin staining in lysed erythrocytes. These hemoglobin deposits occur naturally as a result of macrophage-mediated clearance of erythrocytes. Using Perls Prussian blue staining, we see a substantial increase in sites of free heme staining, as indicated by the blue areas in Figure 5F. Interestingly, we see staining in the red and white pulp of *SLFN14*$^{K208N/+}$ mice but only red pulp where macrophage clearance occurs in controls. This is also supported by the color difference in heterozygous spleens, which appear significantly darker than *SLFN14*$^{+/+}$ spleens (Figure 5Ai). Here, we hypothesize that erythropoiesis is accelerated to compensate for reduced hemoglobin levels. We suggest that *SLFN14*$^{K208N/+}$ erythrocytes are more prone to hemolysis and that the spleen acts as a secondary site of hematopoiesis, specifically upregulating erythropoiesis. The spleen also acts in cell clearance; as such, it may be unable to recognize the need for these additional erythrocytes in oxygen transport which, in the case of *SLFN14*$^{K208N/+}$ mice, may also be the cause of accelerated hemolysis.

Bone marrow profiles showed significant alterations in erythroid progenitors in *SLFN14*$^{K208N/+}$ mice

The main site of hematopoiesis is the bone marrow; therefore, to assess discrepancies in hematopoiesis or altered progenitor levels

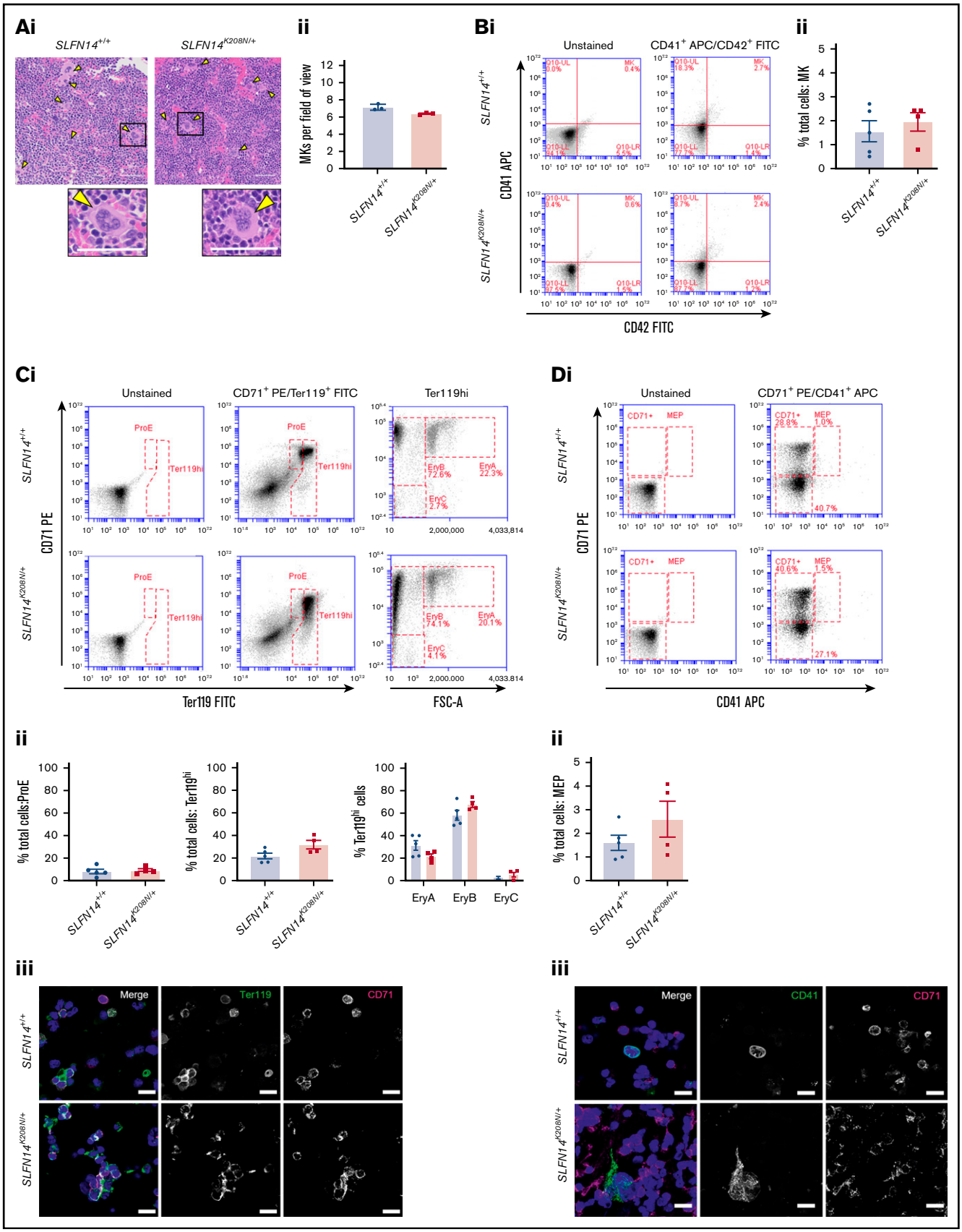
Ai
SLFN14+/+
SLFN14K208N/+
ii
MKs per field of view
Bi
Unstained
CD41+ APC/CD42+ FITC
CD41 APC
CD42 FITC
ii
% total cells: MK
Ci
Unstained
CD71+ PE/Ter119+ FITC
Ter119hi
ProE
EryB
EryA
EryC
CD71 PE
Ter119 FITC
FSC-A
Di
Unstained
CD71+ PE/CD41+ APC
MEP
CD41 APC
ii
% total cells:ProE
% total cells: Ter119hi
% Ter119hi cells
% total cells: MEP
iii
Merge
Ter119
CD71
CD41

Figure 6.

leading to differences in platelet and erythrocyte counts, we examined bone marrow sections and flow cytometry panels, staining for progenitors. Double-blinded evaluation of bone marrow histology sections revealed that MKs were highly populated within the bone marrow, with morphology, including the characteristic polyploid nuclei, consistent across the 2 genotypes (Figure 6A). We analyzed progenitor levels in flushed whole bone marrow from mouse femurs and tibias by flow cytometry. Live single cells were selected based on size and forward scatter to detect progenitor cells and subsequent double-positive populations (determined by antibody staining) gated for analysis (supplemental Figure 2). MKs were highlighted by $CD41^{+}/CD42^{+}$ events (MK quadrant); no difference in the percentage of MKs was observed between genotypes (Figure 6B).

Using CD71 and Ter119 as before, there was no significant difference in the proportion of ProEs in the bone marrow (Figure 6Ci-ii). The percentage of $Ter119^{hi}$ cells was consistent between *SLFN14*$^{K208N/+}$ and wild-type mice; within this population, EryA, EryB, and EryC populations were also unchanged between genotypes (Figure 6Ci-ii). As in spleens, we observed the similar "spread distribution" of variable CD71 expression within the EryB gate; however, in contrast, mature erythrocytes (EryC) were rare. Confocal imaging of this staining pattern is shown in Figure 6Cii.

The predecessor to MKs and ProEs is the MEP. Given the differences that we observed in erythroid cell distribution (Figure 6C) and evidence suggestive of a platelet defect in our patient data, we detected megakaryocyte-erythroblast (MK-EB)–primed MEPs using CD71 and CD41, as before. These double-positive primed MEPs are often difficult to detect in situ within the bone marrow (Figure 6Di).[26] We did not observe any difference in the proportion of $CD71^{+}/CD41^{+}$ cells in *SLFN14*$^{K208N/+}$ mice (Figure 6Dii). Confocal imaging supports an increase in cellular events in the double-positive channel of heterozygotes and more $CD71^{+}$ single-stained events (Figure 6Diii). The reason for this shift in the MEP population is yet to be determined; however, we hypothesize that it results from *SLFN14*$^{K208N/+}$ MK-EB MEPs being more primed in the erythroid direction, consistent with higher single CD71 positivity in this staining panel ($CD71^{+}$; Figure 6Di). Increased $CD71^{+}$ staining may be expansion of the MEP with preference towards the erythroid lineage, as well as due to increased erythroid progenitors after this stage.

SLFN14^{K208N} reduces GATA1 and SLFN14 mRNA levels in hematopoietic cells

To examine whether the K208N mutation led to aberrant expression in hematopoietic cells of *SLFN14*$^{K208N/+}$ mice, we measured the abundance of *SLFN14* mRNA in whole bone marrow by real-time quantitative PCR. Compared with RNA from wild-type controls, *SLFN14* mRNA levels were reduced significantly (by ~50%) in *SLFN14*$^{K208N/+}$ mice ($P < .01$; supplemental Figure 3).

Furthermore, we considered whether levels of the master transcription factor GATA1 were altered as a result of the K208N mutation. Real-time quantitative PCR was performed to measure *GATA1* mRNA levels using cDNA-specific primers for *GATA1* and *GAPDH* as the endogenous control housekeeping gene. *GATA1* levels were reduced substantially in RNA from *SLFN14*$^{K208N/+}$ mice compared with litter-matched controls ($P < .05$; supplemental Figure 3). All primers are given in supplemental Table 5.

Discussion

SLFN14 is a poorly studied endoribonuclease with suspected roles in cleaving RNA that may contribute to a reported thrombocytopenia and clinical bleeding in multiple unrelated patients/families. Here, we present a CRISPR KI mutation of K208N in mice and establish the role of *SLFN14* as a key player in the lineage-commitment pathway, giving rise to species-specific phenotypes in hematopoiesis. In this study, we analyzed heterozygous mutants, because homozygous mutants did not survive to weaning and showed significant deviation from Mendelian inheritance patterns. This suggests that *SLFN14* has a critical role in mouse embryogenesis and, particularly, erythropoiesis. *SLFN14 K208N* is likely to be particularly relevant in future studies of gene-expression profiling in erythrocytes and anemia. E12.5 and E14.5 homozygous embryos were paler than their littermates, showed less distinct vasculature, and did not survive to weaning. These are most likely due to homozygotes' more severe anemia and hemolysis that results in death shortly after birth.[27]

The *K208N* mutation in mice presents with a different phenotype than in its homologous human version, suggesting that it plays a critical role at the MEP junction in lineage fate decisions. Previous studies found that endoribonuclease function is critical in RNA regulation in various bacterial species; however, to our knowledge,

Figure 6. Bone marrow progenitor profile of *SLFN14*$^{K208N/+}$ mice. (Ai) Representative images of H&E-stained femur sections from *SLFN14*$^{K208N/+}$ and *SLFN14*$^{+/+}$ mice. Femurs were fixed in 4% formaldehyde and decalcified before sectioning, staining and quantification of MK number per field of view. MKs are indicated by arrowheads. Scale bars, 50 μm. (Aii) Quantification of MK number per field of view from 3 mice per genotype. Two femurs per mouse were sectioned, and 10 to 13 fields of view per section were quantified blind. Students *t* test was used to assess significance. (B) Quantification of MKs in bone marrow. (Bi) MK staining: MKs were identified by CD41 (αIIb) allophycocyanin (APC) and CD42 (GPIb) fluorescein isothiocyanate (FITC) double staining. (Bii) Quantification of MKs in whole bone marrow by flow cytometry. (C) Quantification of erythroid progenitors in bone marrow. (Ci) ProE staining: ProEs were identified as double-positive CD71 (transferrin receptor 1) phycoerythrin (PE) and Ter119 FITC cells (ProE gate). Maturation of ProEs to mature erythrocytes can be monitored by $Ter119^{hi}$ expression and loss of CD71 expression (EryB and EryC gates). Note the spread of intermediate cells in EryBs, supporting evidence for an altered EryB fate in heterozygotes. (Cii) Quantification of erythroid progenitors in the bone marrow. (Ciii) Confocal images of flow cytometry samples show a double-positive ProE population. Ter119 Alexa Fluor 488 and CD71 Alexa Fluor 647 and DAPI counterstain. Scale bars, 50 μm. (D) Quantification of MEPs in bone marrow. (Di) MK-EB–primed MEPs: MEPs were identified as a small population positive for CD71 (transferrin receptor 1) PE and CD41 (αIIb) APC (MEP). Flow cytometry plots show a slight, but insignificant, increase in MEP cell numbers in SLFN14 K208N mice compared with wild-types. (Dii) MEP quantification in the bone marrow. Staining for these markers highlights MEP cells preferential to the MK or EB lineage. (Diii) Representative images of CD41 Alexa Fluor 488 and CD71 Alexa Fluor 647 stained bone marrow cells imaged by confocal microscopy and using DAPI counterstain. Scale bars, 50 μm. All bone marrow flow cytometry data and quantifications are representative of 4 to 6 mice per genotype/staining condition.

this is the first discovery of endoribonuclease-mediated species differences in mammals.[28,29]

SLFN14^{K219N} patients have a high IPF, suggesting that thrombopoiesis is not sufficient to maintain steady levels of platelet production or that platelet clearance is accelerated. Platelets contain residual RNA from their predecessors, MKs, which form beaded extensions into the lumen of bone marrow sinusoids (proplatelets) and subsequent shear forces of the bloodstream that cause release of preplatelets and platelets into the blood.[30] RNA content can be used to estimate the rate of thrombopoiesis and platelet turnover by measuring the proportion of reticulated platelets within the circulation. An elevated platelet RNA content signifies newer platelets in the circulation that was previously shown to increase platelet reactivity in cardiovascular events and mortality.[31] In the case of *SLFN14*$^{K208N/+}$ mice, we infer that the slight increase in platelet size is due to their immaturity (determined by SYTO13 staining), but this is not accompanied by increased platelet reactivity, as shown in our in vitro and in vivo experiments.

Although no platelet defects were observed in in vitro functional studies, *SLFN14*$^{K208N/+}$ mice exhibited reduced thrombus formation in vivo. These defects in the formation and stability of in vivo thrombi are likely attributable to the abnormal erythrocytes in these mice. Erythrocytes are the primary determinant of blood rheology and promote platelet margination, increasing their concentration near endothelium to enable rapid formation of thrombi in response to vessel damage.[32-34] Indeed, previous studies have shown reduced thrombus formation and extended bleeding times in anemic mice.[35] Although we did not observe altered hemostasis in *SLFN14*$^{K208N/+}$ mice, changes in the size and number of erythrocytes may explain thrombosis findings. Erythrocyte contribution to platelet activation and thrombin generation should also be taken into consideration, together with their unusual role supporting platelet adhesion in the $FeCl_3$ model.[35-37] Although *SLFN14* patients display excessive bleeding phenotypes, we do not report these similarities in mice.[7] Bleeding in *SLFN14* patients has been characterized and explained by defects in platelet aggregation, but little to no effect on platelet function was found in *SLFN14*$^{K208N/+}$ mice. We believe that this work precedes what is to become extensive research into platelet-erythrocyte interactions in health and disease and reveals potential novel mechanisms in hemolysis and anemia.

In *SLFN14*$^{K208N/+}$ mice, we understand that the spleen acts as a secondary site for erythropoiesis. Here, intermediate progenitors (EryBs) differentiate into mature erythrocytes (EryCs), which are highly populated within the spleen. Loss of CD71 expression is indicative of erythrocyte maturation, and the "spread" appearance of EryB cells in heterozygotes clearly shows this maturation phase. This enhanced erythropoiesis is likely due to severe anemia and hemolysis in these mice attempting to compensate for lower hemoglobin levels. The following questions then arise: at what stage in hematopoiesis do *SLFN14* and its mutations cause a shift in lineage commitment to platelet or erythroid directions and how, as an endoribonuclease, does *SLFN14* mediate this transition? Our bone marrow flow cytometry data did not show any difference in bone marrow MK, ProE, or MEP numbers, but there are discrepancies within progenitors of the erythroid lineage suggesting that, in hematopoiesis, *SLFN14*$^{K208N/+}$ leads to altered erythropoiesis and defects in erythroid cells. In the bone marrow, *SLFN14*$^{K208N/+}$ Ter119^{hi} cells expressing CD71 also showed variable expression within the EryB gate, whereas wild-type cells present a more clustered distribution. Platelets and erythrocytes originate from a common progenitor; therefore, pinpointing the exact location of this shift is notoriously difficult. However, we believe that using RNA-sequencing of *SLFN14* progenitors (MKs, ProEs, and MK/EB-MEPs) will reveal discrepancies in RNA expression profiles to support our preliminary findings that a reduction in *GATA1* mRNA is specifically involved in erythroid development. Future work will establish the mechanistic effects of these mutations on human and murine RNA signatures that are critical in lineage commitment. This will uncover novel insights into *SLFN14*'s ability to cleave RNAs which perturb RNA metabolism and protein synthesis in MK and erythroid lineages in a species-dependent manner.

Acknowledgments

The authors thank all technicians and staff at Biomedical Services Unit at the University of Birmingham for housing and husbandry of animals used in this study. They also acknowledge Pip Nicolson for expertise in whole blood smear analysis.

Work in the authors' laboratories is supported by grants from the British Heart Foundation (PG/16/103/32650, FS/18/11/33443) (N.V.M.) and National Institutes of Health, National Institute of General Medical Sciences grant GM097014 (A.V.P.) and National Heart, Lung, and Blood Institute grant HL146544 (A.V.P. and N.V.M.).

Authorship

Contribution: R.J.S., C.W.S., A.O.K., and N.V.M. designed the study, designed and performed experiments, and wrote the manuscript; A.B. generated CRISPR mouse colonies; E.J.H. and S.L. contributed to mouse colony maintenance and experiments; V.P.P., A.V.P., and S.P.W contributed intellectually to the study; and all authors reviewed the manuscript.

Conflict-of-interest disclosure: The authors declare no competing financial interests.

ORCID profiles: R.J.S., 0000-0002-0027-9158; S.L., 0000-0002-0248-8973; S.P.W., 0000-0002-7846-7423; A.O.K., 0000-0003-0825-3179; N.V.M., 0000-0001-6433-5692.

Correspondence: Neil V. Morgan, Institute of Cardiovascular Sciences, College of Medical and Dental Sciences, University of Birmingham, Edgbaston B15 2TT, United Kingdom; e-mail: n.v.morgan@bham.ac.uk.

References

1. Yang J-Y, Deng X-Y, Li Y-S, et al. Structure of Schlafen13 reveals a new class of tRNA/rRNA- targeting RNase engaged in translational control. *Nat Commun*. 2018;9(1):1165.

2. Stapley RJ, Pisareva VP, Pisarev AV, Morgan NV. *SLFN14* gene mutations associated with bleeding. *Platelets*. 2020;31(3):407-410.

3. Geserick P, Kaiser F, Klemm U, Kaufmann SHE, Zerrahn J. Modulation of T cell development and activation by novel members of the Schlafen (slfn) gene family harbouring an RNA helicase-like motif. *Int Immunol*. 2004;16(10):1535-1548.
4. Neumann B, Zhao L, Murphy K, Gonda TJ. Subcellular localization of the Schlafen protein family. *Biochem Biophys Res Commun*. 2008;370(1):62-66.
5. Bustos O, Naik S, Ayers G, et al. Evolution of the Schlafen genes, a gene family associated with embryonic lethality, meiotic drive, immune processes and orthopoxvirus virulence. *Gene*. 2009;447(1):1-11.
6. Schwarz DA, Katayama CD, Hedrick SM. Schlafen, a new family of growth regulatory genes that affect thymocyte development. *Immunity*. 1998;9(5): 657-668.
7. Fletcher SJ, Johnson B, Lowe GC, et al; UK Genotyping and Phenotyping of Platelets study group. SLFN14 mutations underlie thrombocytopenia with excessive bleeding and platelet secretion defects. *J Clin Invest*. 2015;125(9):3600-3605.
8. Marconi C, Di Buduo CA, Barozzi S, et al. SLFN14-related thrombocytopenia: identification within a large series of patients with inherited thrombocytopenia. *Thromb Haemost*. 2016;115(5):1076-1079.
9. Saes JL, Simons A, de Munnik SA, et al. Whole exome sequencing in the diagnostic workup of patients with a bleeding diathesis. *Haemophilia*. 2019; 25(1):127-135.
10. Almazni I, Stapley RJ, Khan AO, Morgan NV. A comprehensive bioinformatic analysis of 126 patients with an inherited platelet disorder to identify both sequence and copy number genetic variants. *Hum Mutat*. 2020;41(11):1848-1865.
11. Khan AO, Stapley RJ, Pike JA, et al; UK GAPP Study Group. Novel gene variants in patients with platelet-based bleeding using combined exome sequencing and RNAseq murine expression data. *J Thromb Haemost*. 2021;19(1):262-268.
12. Fletcher SJ, Pisareva VP, Khan AO, Tcherepanov A, Morgan NV, Pisarev AV. Role of the novel endoribonuclease SLFN14 and its disease-causing mutations in ribosomal degradation. *RNA*. 2018;24(7):939-949.
13. Magella B, Adam M, Potter AS, et al. Cross-platform single cell analysis of kidney development shows stromal cells express Gdnf. *Dev Biol*. 2018;434(1): 36-47.
14. Olsson A, Venkatasubramanian M, Chaudhri VK, et al. Single-cell analysis of mixed-lineage states leading to a binary cell fate choice [published correction appears in *Nature*. 2019;569(7715):E3]. *Nature*. 2016;537(7622):698-702.
15. Lu YC, Sanada C, Xavier-Ferrucio J, et al. The molecular signature of megakaryocyte-erythroid progenitors reveals a role for the cell cycle in fate specification[published correction appears in *Cell Rep*. 2018;25(11):3229]. *Cell Rep*. 2018;25(8):2083-2093.e4.
16. Pisareva VP, Muslimov IA, Tcherepanov A, Pisarev AV. Characterization of novel ribosome-associated endoribonuclease SLFN14 from rabbit reticulocytes. *Biochemistry*. 2015;54(21):3286-3301.
17. Mills EW, Wangen J, Green R, Ingolia NT. Dynamic regulation of a ribosome rescue pathway in erythroid cells and platelets. *Cell Rep*. 2016;17(1):1-10.
18. Khan AO, Maclachlan A, Lowe GC, et al. High-throughput platelet spreading analysis: a tool for the diagnosis of platelet- based bleeding disorders. *Haematologica*. 2020;105(3):e124-e128.
19. Pike JA, Simms VA, Smith CW, et al. An adaptable analysis workflow for characterization of platelet spreading and morphology. *Platelets*. 2020;Apr 23: 1-5.
20. Tucker KL, Sage T, Gibbins JM. Clot retraction. *Methods Mol Biol*. 2012;788:101-107.
21. Smith CW, Raslan Z, Parfitt L, et al. TREM-like transcript 1: a more sensitive marker of platelet activation than P-selectin in humans and mice. *Blood Adv*. 2018;2(16):2072-2078.
22. Hille L, Cederqvist M, Hromek J, Stratz C, Trenk D, Nührenberg TG. Evaluation of an alternative staining method using SYTO 13 to determine reticulated platelets. *Thromb Haemost*. 2019;119(5):779-785.
23. Crow AR, Lazarus AH. Role of Fcgamma receptors in the pathogenesis and treatment of idiopathic thrombocytopenic purpura. *J Pediatr Hematol Oncol*. 2003;25(suppl 1):S14-S18.
24. Mori J, Nagy Z, Di Nunzio G, et al. Maintenance of murine platelet homeostasis by the kinase Csk and phosphatase CD148. *Blood*. 2018;131(10): 1122-1144.
25. Koulnis M, Pop R, Porpiglia E, Shearstone JR, Hidalgo D, Socolovsky M. Identification and analysis of mouse erythroid progenitors using the CD71/ TER119 flow-cytometric assay. *J Vis Exp*. 2011;(54):2809.
26. Psaila B, Barkas N, Iskander D, et al. Single-cell profiling of human megakaryocyte-erythroid progenitors identifies distinct megakaryocyte and erythroid differentiation pathways. *Genome Biol*. 2016;17(1):83.
27. Baron MH, Vacaru A, Nieves J. Erythroid development in the mammalian embryo. *Blood Cells Mol Dis*. 2013;51(4):213-219.
28. Trinquier A, Durand S, Braun F, Condon C. Regulation of RNA processing and degradation in bacteria. *Biochim Biophys Acta Gene Regul Mech*. 2020; 1863(5):194505.
29. Mardle CE, Shakespeare TJ, Butt LE, et al. A structural and biochemical comparison of Ribonuclease E homologues from pathogenic bacteria highlights species-specific properties. *Sci Rep*. 2019;9(1):7952.
30. Machlus KR, Italiano JE Jr.. The incredible journey: from megakaryocyte development to platelet formation. *J Cell Biol*. 2013;201(6):785-796.
31. Grove EL, Hvas A-M, Kristensen SD. Immature platelets in patients with acute coronary syndromes. *Thromb Haemost*. 2009;101(01):151-153.
32. Byrnes JR, Wolberg AS. Red blood cells in thrombosis. *Blood*. 2017;130(16):1795-1799.
33. Turitto VT, Baumgartner HR. Platelet interaction with subendothelium in a perfusion system: physical role of red blood cells. *Microvasc Res*. 1975;9(3): 335-344.

34. Turitto VT, Weiss HJ. Red blood cells: their dual role in thrombus formation. *Science*. 1980;207(4430):541-543.

35. Klatt C, Krüger I, Zey S, et al. Platelet-RBC interaction mediated by FasL/FasR induces procoagulant activity important for thrombosis. *J Clin Invest*. 2018;128(9):3906-3925.

36. Barr JD, Chauhan AK, Schaeffer GV, Hansen JK, Motto DG. Red blood cells mediate the onset of thrombosis in the ferric chloride murine model. *Blood*. 2013;121(18):3733-3741.

37. Woollard KJ, Sturgeon S, Chin-Dusting JP, Salem HH, Jackson SP. Erythrocyte hemolysis and hemoglobin oxidation promote ferric chloride-induced vascular injury. *J Biol Chem*. 2009;284(19):13110-13118.